Heliyon 10 (2024) e39258

Contents lists available at ScienceDirect

Heliyon

journal homepage: www.cell.com/heliyon

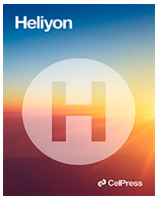

Research article

Construction and experimental verification of a novel nine-glycosylation-related gene prognostic risk model for clear cell renal carcinoma

Wanlei Sun [a], Long Guo [b], Jianqing Ye [a], Min Zhou [b], Cong Shu [b], Xin Ying [b], Hongliang Liu [c], Fei Liu [b,*]

[a] Department of Clinical Laboratory, the Second Affiliated Hospital of Nanchang University, Nanchang, China
[b] Department of Urology, the Second Affiliated Hospital of Nanchang University, Nanchang, 330006, Jiangxi Province, China
[c] Department of General surgery, the Second Affiliated Hospital of Nanchang University, Nanchang, China

ARTICLE INFO

Keywords:
Clear cell renal carcinoma
Glycosylation modification
Prognostic signature
Risk model
Immune cell infiltration

ABSTRACT

Objective: Patients with clear cell renal carcinoma (ccRCC) typically have poor prognosis. Glycosylation modification plays an important role in ccRCC. This study aimed to develop a novel signature for predicting ccRCC prognosis based on glycosylation-related genes (GRGs).
Methods: Differentially expressed GRGs (DE_GRGs) were identified using The Cancer Genome Atlas (TCGA) and Gene Expression Omnibus and used for constructing the risk model. The function of key genes was validated.
Results: Twenty-two DE_GRGs were intersected between GSE53757 and TCGA. Patients with ccRCC were divided into two clusters based on the expression profile of these DE_GRGs. Significant differences in the infiltration of 10 immune cell types were observed between two subclusters. Subsequently, the prognostic signatures of nine DE_GRGs (CHST9, COLGALT1, FUT3, FUT6, HS3ST2, POMGNT2, ST8SIA4, UGT3A1, and UGT8) were established. Patients in the high-risk group showed a poorer prognosis relative to the low-risk group. According to univariate and multivariate Cox regression analyses, the risk score, stage, and grade could be independent prognostic factors. A nomogram incorporating information on gender, age, risk group, TNM stage, and clinical stage showed accurate prediction in the survival probability. Except for CHST9, HS3ST2, and ST8SIA4, expression patterns of the remaining 6 DE_GRGs in Caki-1 and 786-O cells were confirmed by quantitative real-time PCR. FUT6 overexpression resulted in the inhibition of proliferation, migration, and invasion of ccRCC cells.
Conclusion: This study established a nine-DE_GRG-based prognostic signature, which independently predicted ccRCC prognosis. This finding emphasizes that GRGs are stratification factors for the precise prognosis of ccRCC.

1. Introduction

Clear cell renal carcinoma (ccRCC), which originates from renal cortical or tubular epithelial cells, is the predominant histological

* Corresponding author. Department of Urology, the Second Affiliated Hospital of Nanchang University, No. 1 Min De Road, Nanchang, Jiangxi Province, 330006, China.
E-mail address: lu312519@126.com (F. Liu).

https://doi.org/10.1016/j.heliyon.2024.e39258
Received 23 June 2024; Received in revised form 20 September 2024; Accepted 10 October 2024
Available online 11 October 2024

Abbreviations

ccRCC	clear cell renal carcinoma
GRGs	glycosylation-related genes
DE_GRGs	differentially expressed GRGs
OS	overall survival
KIRC	kidney renal clear cell carcinoma
TCGA	The Cancer Genome Atlas
FDR	false discovery rate
CDF	cumulative distribution function
t-SNE	t-distributed random neighbor embedding
LASSO	Least Absolute Shrinkage and Selection Operator
ROC	receiver operating characteristic
RT-qPCR	quantitative real-time polymerase chain reaction
CCK-8	cell counting kit-8

subtype of renal carcinoma, comprising approximately 75%–80 % of cases [1,2]. ccRCC ranks as the seventh most common cancer of genitourinary system in men with a high mortality rate [3]. Approximately 64,000 cases and up to 14,000 deaths are reported in the United States each year, and the incidence peaks at ages 60 to 80 [3,4]. Currently, surgical resection remains the cornerstone of ccRCC therapy; however, the incidence of recurrence and metastasis following surgery can be as high as 30%–35 % among patients [5]. Therefore, it is important to reasonably assess the prognosis of ccRCC patients. Models based on multiple genes associated with disease progression play an important role in predicting the prognosis of many cancers [6,7]. Therefore, it is important to construct an effective and stable prognostic model of gene sets for ccRCC.

Glycosylation is one of the most common and complex of post-translational modifications. The combination of large amounts of naturally occurring sugars with lipid and protein molecules to form a variety of unique glycan structures is known as glycosylation [8,9]. Humans have six major types of protein glycosylation, including the addition of phosphorylated glycans, N-, O-, C- linked glycans, glycosaminoglycans and glycosylphosphatidylinositol anchors [10]. Protein glycosylation not only greatly facilitates the expansion of proteome, beyond the scope of genome coding, but also had a far-reaching impact on protein stability, subcellular localization, function, and other traits [11]. Altered glycosylation plays a crucial role in cancer development and progression, and some glycosylated structures are typical markers of tumor progression [12,13]. GALNT6 accelerated breast cancer metastasis by augmenting mucin type O-glycosylation of α2M [14]. GALNT14-controlled O-glycosylation at serine-161 of PHB2 promoted hepatoma cell proliferation, migration, and drug resistance through the activation of IGF1R cascade [15]. Moreover, upregulated β4GalT-II was positively correlated with clinical features in non-metastatic ccRCC patients and regulated the tumor development and dissemination [16]. The high expression of ST6GaNAc-1 is associated with the overall survival (OS) of patients with nonmetastatic ccRCC [17]. Therefore, the construction of prognostic models for ccRCC based on glycosylation genes is of great value.

In this study, we developed a new prognostic signature based on glycosylation genes to predict the prognosis of patients with

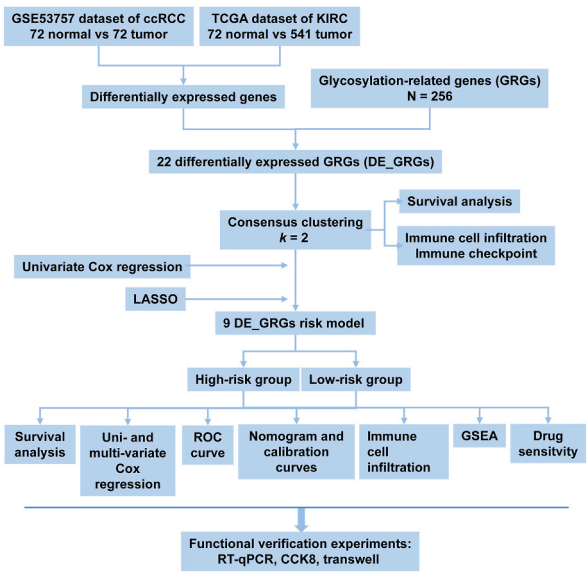

Fig. 1. Comprehensive flow chart of the study design.

ccRCC. Our study helps further the understanding of the role of glycosylation modifications in ccRCC progression and provides clues for the development of targeted prognostic prediction and treatment strategies.

2. Materials and methods

2.1. Data collection and processing

Fig. 1 shows a comprehensive flow chart of the study design. We downloaded expression data for kidney renal clear cell carcinoma (KIRC) from The Cancer Genome Atlas (TCGA), which comprised 72 normal tissues and 541 tumor tissues. The expression data were processed and normalized using log 2(TPM + 1) transformation before differential expression analysis. The microarray expression profile data (GSE53757) of 72 tumor tissues and 72 normal tissues were downloaded from Gene Expression Omnibus, which uses the GPL570 [HG-U133_Plus_2] Affymetrix Human Genome U133 Plus 2.0 Array platform. The complete list of glycosylation-related genes (GRGs) was downloaded from https://acgg.asia/ggdb2/index, and 256 GRGs were obtained (Supplemental Table 1). Based on these 256 GRGs, differentially expressed GRGs (DE_GRGs) were identified in TCGA and GSE53757 datasets using limma package (version 3.56.2) with a screening threshold of logFC $\geq$1 and false discovery rate (FDR) $<$ 0.05. Twenty-two DE_GRGs related to glycosylation in ccRCC were intersected between the two datasets.

2.2. Consensus clustering analysis of DE_GRGs

Based on the 22 DE_GRGs, consensus clustering was carried out with a maximum *k*-value of 9 using "ConsensusClusterPlus" R package to separate the ccRCC samples into different clusters upon 1000 bootstraps and "pam" cluster algorithm. We analyzed the consensus cumulative distribution function (CDF) curve and relative change of the area under the CDF curve to obtain the optimal cluster number. Moreover, we performed t-distributed random neighbor embedding (t-SNE) analysis utilizing the "Rtsne" R package.

2.3. Immune cell infiltration

The infiltration ratios of 22 immune cells in each sample were calculated through deconvolution algorithms using the CIBERSORT package (version 0.1.0) and signatures for 22 types of immune cells. The ggplot2 package (version 3.4.3) was used to create boxplots to compare the cell ratios between the two clusters. Differential expression analysis of 36 immune checkpoint genes between the two clusters was performed using limma package with FDR $<$0.05.

2.4. Establishment of the GRG-based prognostic risk model

Univariate Cox regression analysis was used to determine the potential of 22 DE_GRGs in predicting the prognosis of patients with ccRCC, and the hazard ratios were obtained. DE_GRGs with p-values less than 0.01 were used in the Least Absolute Shrinkage and Selection Operator (LASSO) regression analysis, and the number of DE_GRGs in the final risk model was determined using the "glmnet" R package. The risk model refracts both the expression levels of the nominated DE_GRGs and their relative regression coefficient weights calculated from univariate Cox regression analysis. The risk model was calculated using the prognostic signature of DE_GRGs through the following formula: risk model = (coefficient $\times$ the expression of DE_GRG_1) + (coefficient $\times$ the expression of DE_GRG_2) + (coefficient $\times$ the expression of DE_GRG_3) + … + (coefficient $\times$ the expression of DE_GRG_n). In light of the median risk score of all samples, the patients were categorized into high- and low-risk groups. Next, the "survival" R package was used to conduct survival analysis of both groups and to create the survival curve, scatterplot, and expression heat map.

2.5. Prognostic value analysis of the risk score

Univariate and multivariate Cox regression analyses were used to determine whether the DE_GRGs risk model served as an independent prognostic factor for patients with ccRCC. The "survivalROC" R package was used to draw receiver operating characteristic (ROC) curves for 1-, 3-, and 5-year OS rates in patients with ccRCC in order to evaluate the accuracy of the risk score model. Moreover, we established a nomogram using the "rms" R package to predict the survival of patients with ccRCC based on statistically significant clinicopathological characteristics (gender, TNM stage, age) in the ROC curves. Calibration curves were generated using the "ggDCA" R package to evaluate the concordance between actual survival and the nomogram's prediction results.

2.6. Drug response of ccRCC samples

The "oncoPredict" R package was utilized to predict the drug response of ccRCC samples in the high- and low-risk groups. Limma package was utilized to figure the half-maximal inhibitory concentration (IC_{50}), and boxplots were created using the "ggplot2" package. The Wilcoxon signed-rank test was used to determine the statistical significance of drug sensitivity between the high- and low-risk groups.

2.7. Cell culture and transfection

Human renal cortex proximal tubule epithelial cell line HK-2 (iCell-h096) and human renal cancer cell lines 786-O (iCell-h235) and Caki-1 (iCell-h040) were acquired from iCell. The cells were cultured in RPMI 1640 medium (Corning, 10-040-CVRC) containing 10 % fetal bovine serum and 1 % penicillin/streptomycin (E607011, Sangon, China) in a 5 % CO_2 incubator at a constant temperature of 37 °C.

To overexpress FUT6, the full length of FUT6 was constructed into the pcDNA3.1 vector and then transfected into Caki-1 and 786-O cells using Lipofectamine 2000 (Invitrogen) reagents.

2.8. Quantitative real-time polymerase chain reaction (RT-qPCR) analysis

RNA was extracted using TRIzol Reagent (Invitrogen), and the RNA quality was assessed using a microspectrophotometer and agarose gel electrophoresis. Next, RNA was reverse transcribed into cDNA utilizing the RevertAid First Strand cDNA Synthesis Kit (#K1622, Thermo). RT-qPCR analysis was conducted using 2 × Master Mix (Roche) on an ABI Q6 PCR system (Applied Biosystems Inc, USA). PCR was performed with initial denaturation at 95 °C for 10 min, followed by 45 cycles of denaturation at 95 °C for 15 s and annealing at 60 °C for 60 s. Gene expression was determined using the $2^{-\Delta\Delta Ct}$ method. Primer sequences are listed in Supplemental Table 2.

2.9. Cell Counting Kit-8 (CCK-8) assays

After the FTU6 overexpression plasmid was transfected into 786-O and Caki-1 cells for 6 h, the cells were digested using trypsin (25,200,072, GIBCO), and the cell concentration was adjusted to 1×10^4/mL. About 1000 cells were spread in each well, and six replicate wells were established for each sample. The cells were cultured for 0, 24, 48, 72, and 96 h and then added with 10 μL of CCK-8 solution. After 1 h, the optical density value was measured at 450 nm on a microplate reader (Infinite M1000, TECAN).

2.10. Transwell assays

Following transfection with the FTU6 overexpression plasmid for 24 h, 786-O and Caki-1 cells were digested using trypsin (25,200,072, GIBCO), and the cell concentration was standardized to 1×10^5/mL. For cell migration assays, 24-well plate chambers (8 μm, 353097, FALCON) were used. For cell invasion assays, BioCoat™ Matrigel® 24-well plate chambers (8 μm, 354480, BioCoat) were used. Approximately 700 μL of medium containing 20 % serum was added to the lower chamber (the bottom of the 24-well plate), and

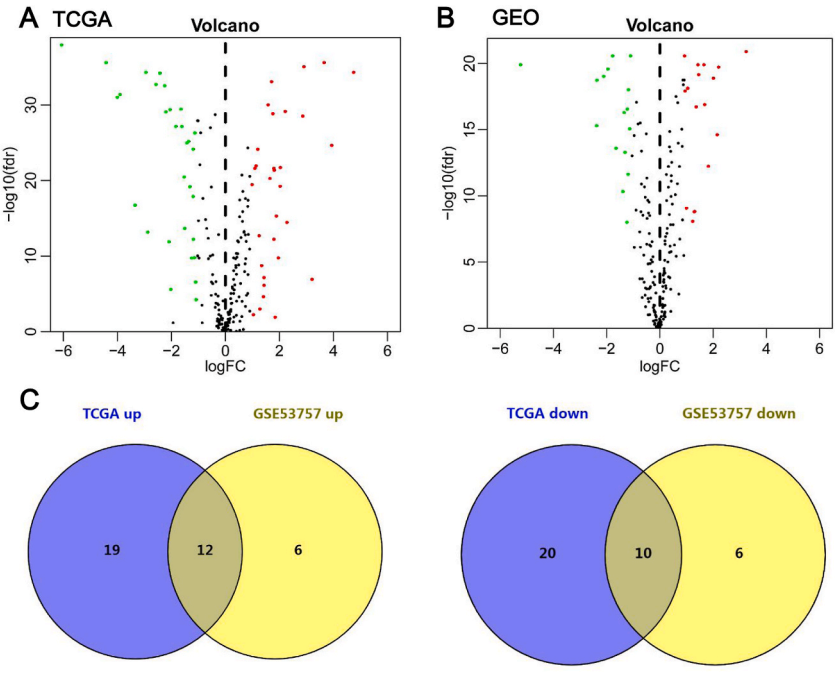

Fig. 2. Identification of DE_GRGs in ccRCC.
(A) Volcano plot of differentially expressed glycosylation-related genes (DE_GRGs) between normal tissues (n = 72) and tumor tissues (n = 541) of KIRC in TCGA database. (B) Volcano plot of DE_GRGs between normal tissues (n = 72) and tumor tissues (n = 72) of ccRCC in GSE53757. (C) The intersection of the upregulated and downregulated DE_GRGs in the GSE53757 and TCGA results.

500 μL of cell suspension was added to the upper chamber. Afterward, incubation was continued for 48 h. Next, the lower chamber was transferred into wells containing 800 μL of paraformaldehyde and fixed for 30 min. Subsequently, the chamber was incubated with 800 μL of crystal violet solution for 30 min. The chamber was gently washed with water for several times and sealed with neutral gum. Three random fields of view were imaged under a microscope (XSP-37XB, Shanghai Optical Instrument Factory).

2.11. Statistical analysis

GraphPad Prism 9.0 software was used for statistical analysis and data graphing. The *t*-test was applied for comparison between two groups, and statistical significance was considered at $p < 0.05$.

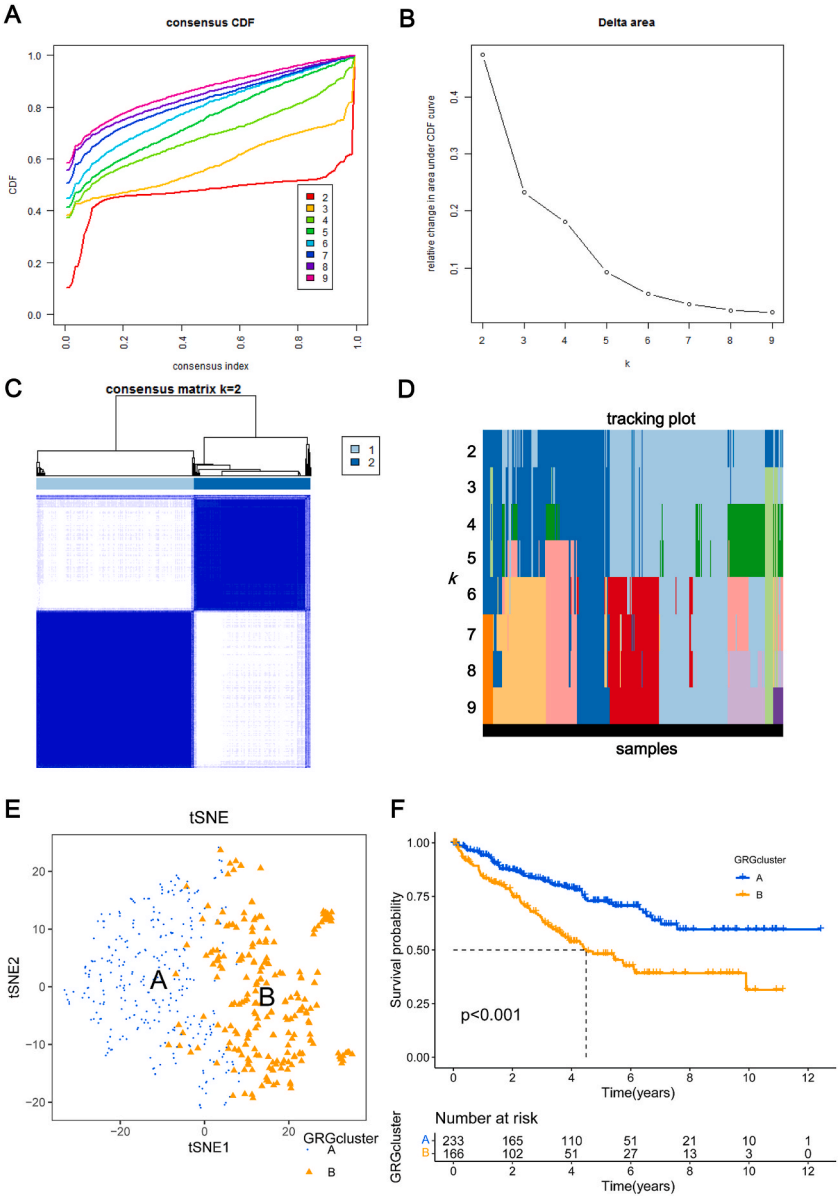

Fig. 3. Consensus clustering analysis of ccRCC samples.
(A) Consensus cumulative distribution function (CDF) curve, *k* from 2 to 9. (B) The relative change in area under CDF curve, *k* from 2 to 9. (C) Consensus clustering heat map when $k = 2$. (D) The tracking plot of consensus clustering of *k* from 2 to 9. (E) The distribution of two clusters was verified by t-SNE analysis. (F) Survival analysis between the two clusters.

3. Results

3.1. Identification of DE_GRGs in ccRCC

To identify DE_GRGs, we performed screening using the GSE53757 dataset (72 normal tissues vs. 72 tumor tissues) and TCGA database (72 normal tissues vs. 541 tumor tissues) with a screening threshold of logFC $\geq$1 and FDR $<$0.05. We determined 34 (16 upregulated and 18 downregulated) and 61 (30 upregulated and 31 downregulated) DE_GRGs, respectively, based on the GRG lis t (Fig. 2A and B, fig. S1). Subsequently, the intersection of DE_GRGs in the GSE53757 and TCGA results was taken, and 22 DE_GRGs were finally obtained, including 12 upregulated and 10 downregulated DE_GRGs in ccRCC tumor tissues compared with normal tissues (Fig. 2C). Therefore, 22 DE_GRGs were used in the subsequent analysis.

3.2. Consensus clustering analysis and immune infiltration landscape analysis

We performed consensus clustering analysis using the expression profile of 22 DE_GRGs to reclassify patients with ccRCC into distinct clusters, and we calculated the CDF curve (Fig. 3A) and relative change in area under the CDF curve (Fig. 3B) to obtain the optimal cluster number. As a result of consensus clustering analysis $k = 2$ determined as the optimal cluster number, displaying relative stability, when the clustering stability datasets varied from $k = 2$ to $k = 9$ (Fig. 3C and D). Cluster A comprised 308 samples, whereas

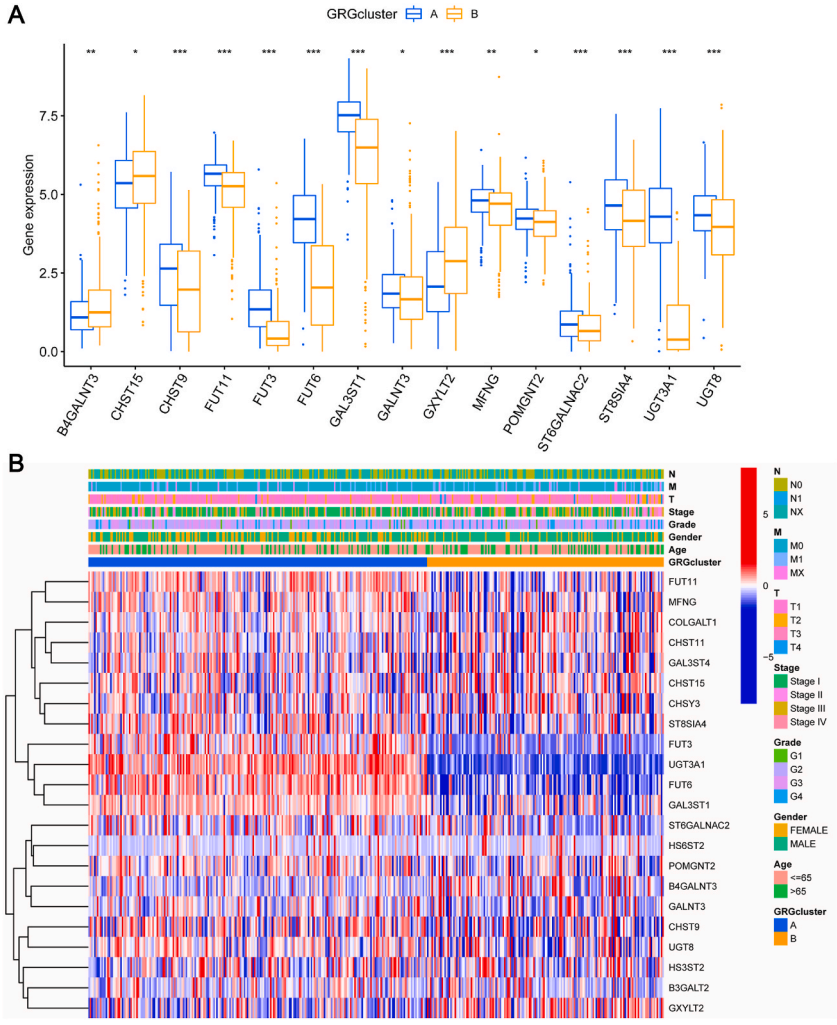

Fig. 4. The distribution of 22 DE_GRGs expression and clinicopathological features in two clusters.
(A) The boxplot of expression of 22 DE_GRGs in Clusters A and B. B4GALNT3, CHST15, CHST9, FUT11, FUT3, FUT6, GAL3ST1, GALNT3, GXYLT2, MFNG, POMGNT2, ST6GALNAC2, ST8SIA4, UGT3A1, and UGT8 were significantly differentially expressed between Cluster A and Cluster B. (B) Heat map presenting the expression distribution of 22 DE_GRGs and clinicopathological features (clinical stage, gender, grade, age, and TNM stage) in Clusters A and B.

Cluster B consisted of 225 samples. The distribution of both clusters was verified by t-SNE analysis. Clusters A and B were obviously distinguished as shown in Fig. 3E. Survival analysis proved that Cluster A had a significantly longer OS than Cluster B (Fig. 3F). Next, the expression of 22 DE_GRGs (FUT11, MFNG, COLGALT1, CHST11, GAL3ST4, CHST15, CHSY3, ST8SIA4, FUT3, UGT3A1, FUT6, GAL3ST1, ST6GALNAC2, HS6ST2, POMGNT2, B4GALNT3, GALNT3, CHST9, UGT8, HS3ST2, B3GALT2, and GXYLT2) in Clusters A and B was calculated, and the boxplot showed that only 15 DE_GRGs were significantly differentially expressed (Fig. 4A). A heat map presented the expression distribution of 22 DE_GRGs in clinicopathological characteristics, including clinical stage, gender, grade, age, and TNM stage (Fig. 4B).

With regard to immunity, notable discrepancies were observed in the infiltration of 10 types of immune cells (including T cells CD8, mast cells resting, dendritic cells resting, T cells CD4 memory activated, T cells gramma delta, monocytes, dendritic cells activated, macrophage M0, macrophage M1, mast cells activated) in Clusters A and B of ccRCC samples (Fig. S2A). All 10 types of immune cells showed a strong correlation with 22 DE_GRGs (Fig. S2B). Among these 10 immune cell types, T cells CD8 showed a positive correlation

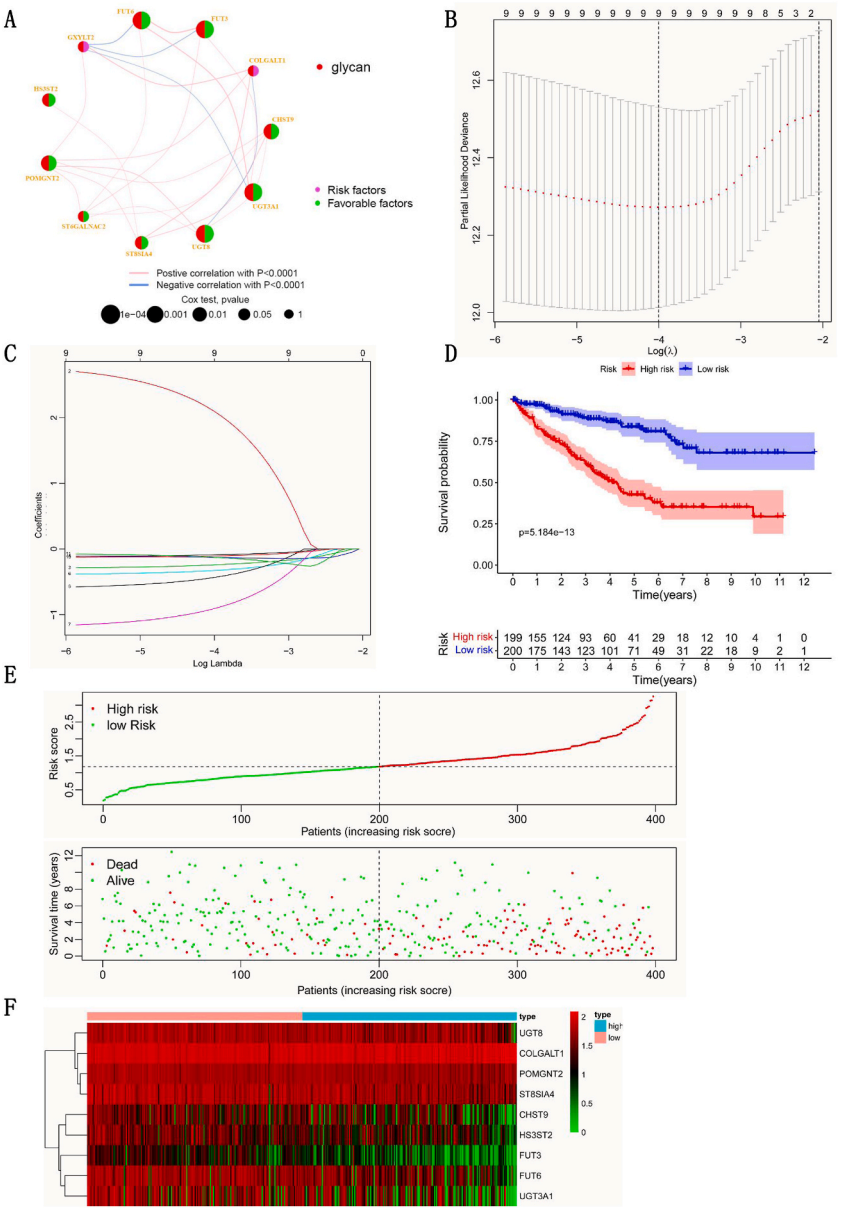

Fig. 5. Generation of the DE_GRG risk model.
(A) Univariate Cox regression analysis of DE_GRGs. (B) Change trajectory of each independent variable. (C) The confidence interval under different lambda values. (D) Survival analysis between high- and low-risk groups. (E) Risk score, survival time, and expression of nine GRGs between high- and low-risk groups in TCGA cohort.

with T cells follicular helper, while exhibiting a negative correlation with T cells CD4 memory resting (Fig. S2C). The other cells showed little correlation with each other. Interestingly, 16 of the 18 immune checkpoint genes were markedly upregulated in Cluster A compared with Cluster B, and only two were reduced in group B (Fig. S2D), suggesting that Cluster A was more susceptible to immunotherapy than Cluster B. These 16 immune checkpoint genes were also significantly associated with 22 DE_GRGs (Fig. S2E). Overall, these 22 DE_GRGs were associated with immune infiltration.

3.3. Generation of a DE_GRGs risk model

According to the results of univariate Cox regression analysis, 11 DE_GRGs were identified as prognostic factors. Among them, nine DE_GRGs (CHST9, FUT3, FUT6, HS3ST2, POMGNT2, ST6GALNAC2, ST8SIA4, UGT3A1, UGT8) with a hazard risk ratio <1 might be protective indicators, whereas the remaining two DE_GRGs (COLGALT1 and GXYLT2) were poor prognostic predictors (Fig. 5A). Next,

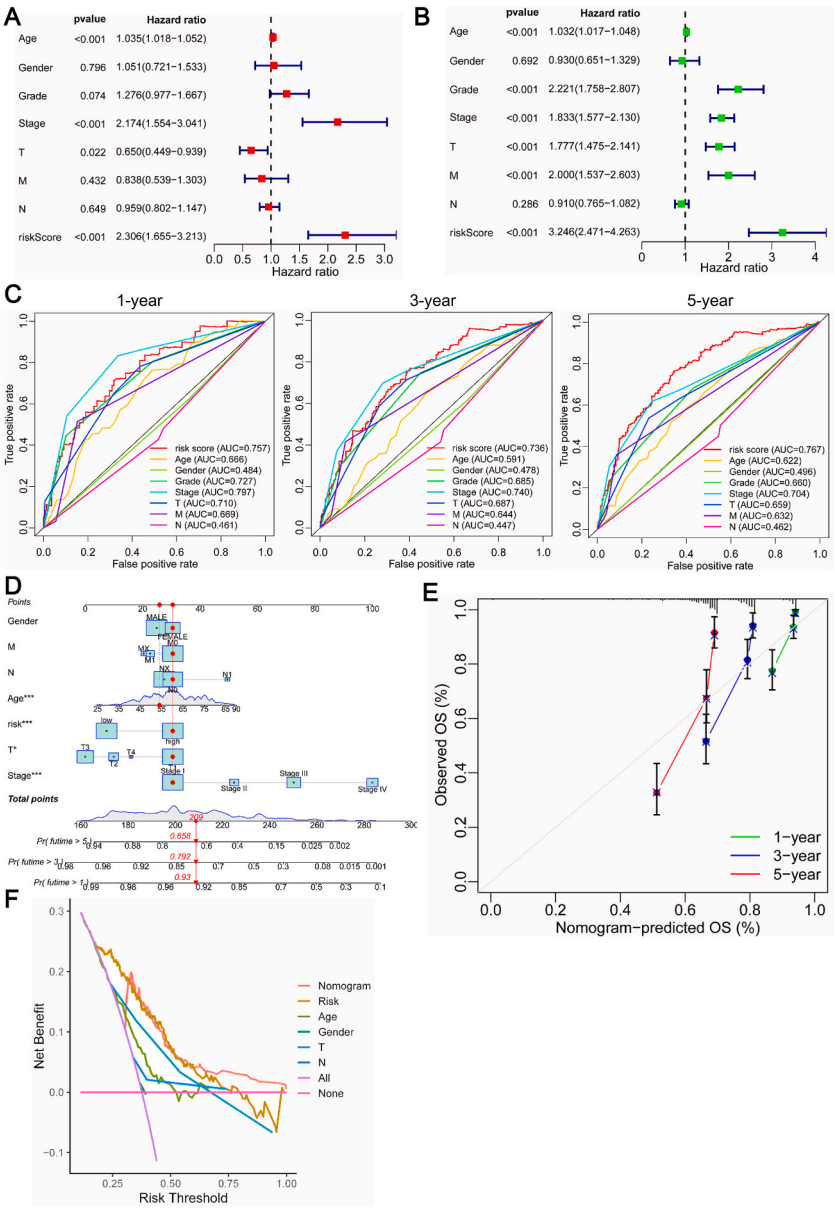

Fig. 6. Establishment of a nomogram for ccRCC patients.
(A) Univariate and (B) multivariate Cox regression analyses were used to assess the risk model. (C) Time-dependent ROC curves of OS (AUCs for 1, 3, and 5 years) in patients with ccRCC in TCGA cohort. (D) Nomogram construction based on the risk model and clinicopathological features. (E) A calibration curve was used to assess the accuracy of the nomogram. (F) Decision curve analysis (DCA) curves of risk scores and clinical characteristics for the TCGA at 5 years.

we conducted LASSO analysis on these 11 DE_GRGs (Fig. 5B and C). The results showed that these nine DE_GRGs were independent prognostic indicators and used to construct the risk model. The risk model was calculated based on the DE_GRGs prognostic signature, utilizing the following formula: risk model = (−0.09027 × the expression of CHST9) + (2.098 × the expression of COLGALT1) + (−0.2434 × the expression of FUT3) + (−0.1293 × the expression of FUT6) + (−0.3287 × the expression of HS3ST2) + (−0.9095 × the expression of POMGNT2) + (−0.4346 × the expression of ST8SIA4) + (−0.1088 × the expression of UGT3A1) + (−0.1288 × the expression of UGT8). In light of the median risk score, patients with ccRCC were separated into high- and low-risk groups in TCGA cohort. We found that the high-risk group had poorer prognosis than the low-risk group (Fig. 5D and E). The expression of nine

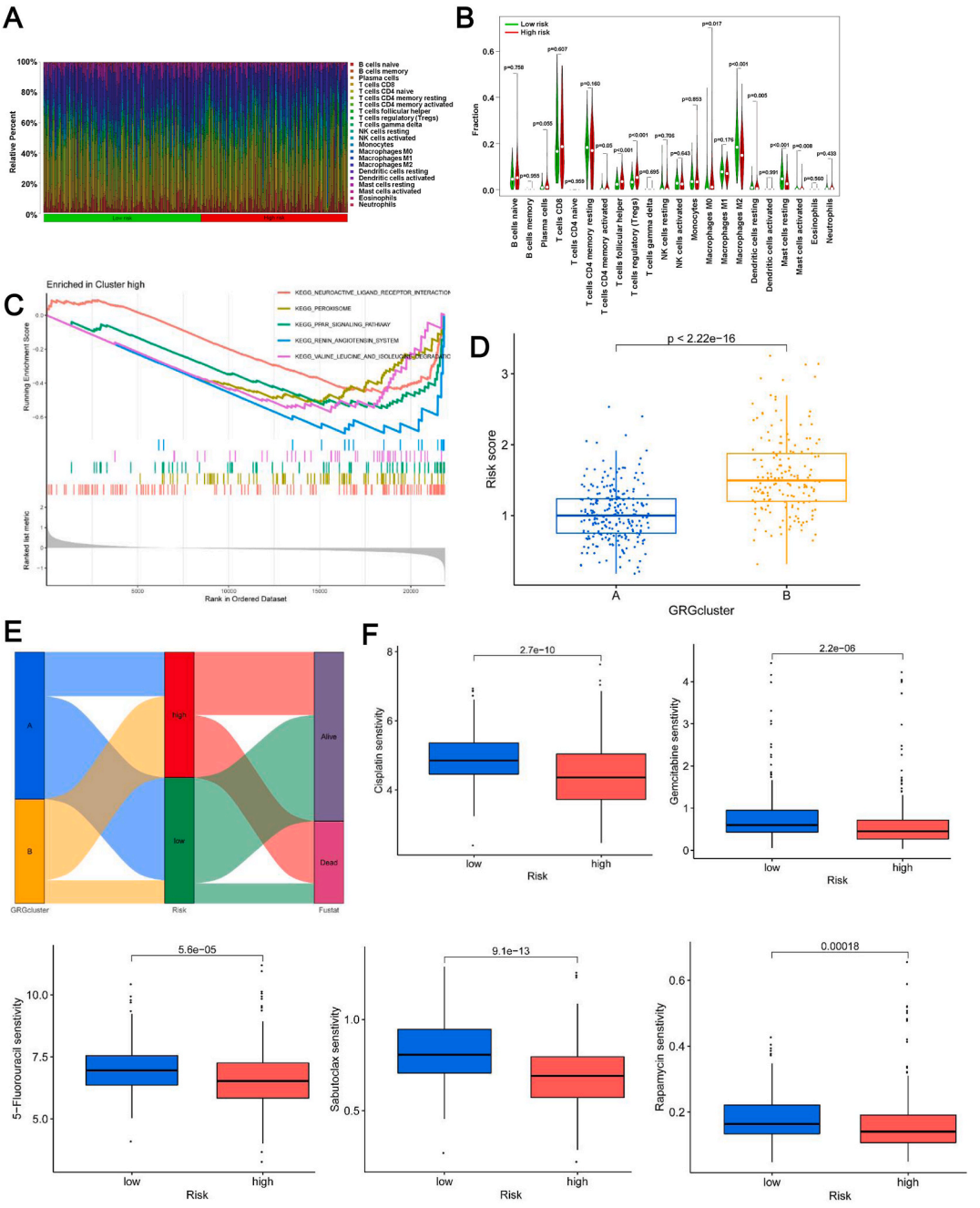

Fig. 7. Immune infiltration and drug sensitivity in the risk groups.
(A) The proportion of various infiltrating immune cells in the high- and low-risk groups. (B) Immune infiltration of different types of immune cells in the high- and low-risk groups. (C) GSEA showed the Kyoto Encyclopedia of Genes and Genomes enrichment pathway of the high-risk group. (D) The risk score of Clusters A and B. (E) Alluvial plot of the relationship between clusters and risk groups. (F) IC_{50} values of cisplatin, gemcitabine, 5-fluorouracil, sabutoclax, and rapamycin in high- and low-risk groups.

DE_GRGs in the risk model is shown in Fig. 5F. Taken together, a novel nine-DE_GRG-related prognostic signature was constructed.

3.4. Establishment of a nomogram for ccRCC patients

Univariate and multivariate Cox regression analyses were performed to determine whether the DE_GRGs risk model provided independent prognostic value for ccRCC patients. The results showed that grade (in univariate: Hazard ratio = 1.276, 95%CI 0.977–1.667, p = 0.074; in multivariate: Hazard ratio = 2.22, 95%CI 1.758–2.807, p < 0.001), stage (in univariate: Hazard ratio = 2.174, 95%CI 1.554–3.041, p < 0.001; in multivariate: Hazard ratio = 1.833, 95%CI 1.577–2.130, p < 0.001), and risk score (in

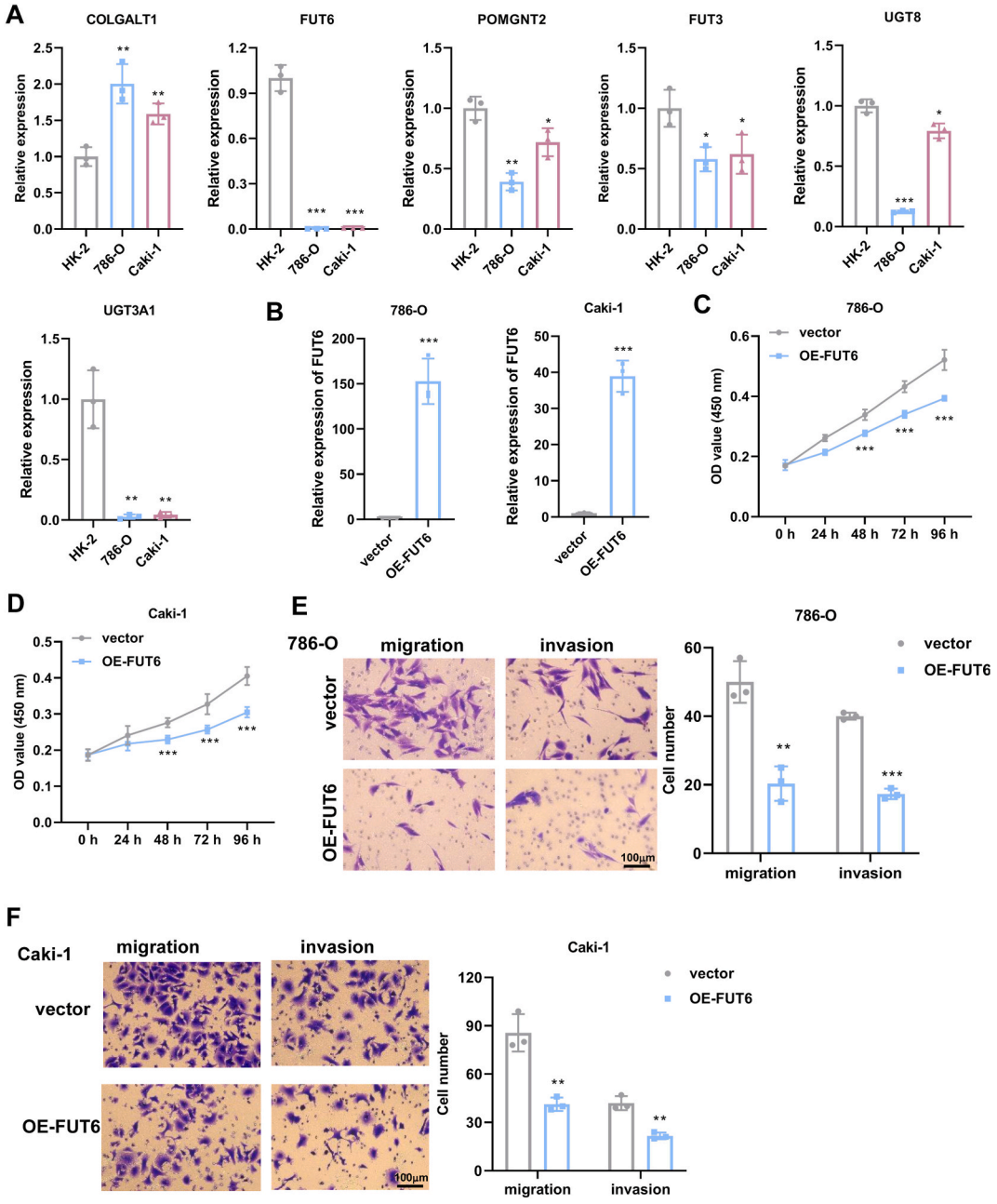

Fig. 8. FUT6 suppressed the proliferation, migration, and invasion of ccRCC cells.
(A) The expression of six DE_GRGs (COLGALT1, FUT3, FUT6, POMGNT2, UGT3A1, and UGT8) in HK-2, 786-O, and Caki-1 cells was verified by RT-qPCR. (B) Overexpression efficiency of FUT6 in 786-O and Caki-1 cells. The proliferation of 786-O (C) and Caki-1 cells (D) after FUT6 overexpression was detected by CCK-8 assays. The migration and invasion of 786-O (E) and Caki-1 cells (F) after FUT6 overexpression were detected by transwell assays. Scale bar: 100 μm *p < 0.05; **p < 0.01; ***p < 0.001.

univariate: Hazard ratio = 2.306, 95%CI 1.855–3.213, $p < 0.001$; in multivariate: Hazard ratio = 3.246, 95%CI 2.471–4.263, $p < 0.001$) could be independent prognostic factors (Fig. 6A and B). Moreover, the time-dependent ROC curves showed that the risk score accurately predicted OS in ccRCC patients within the TCGA cohort, with good performance.

The efficacy of risk score in accurately predicting OS in ccRCC patients in TCGA cohort was good (areas under the ROC curve [AUCs] of 0.757, 0.736, and 0.767 for 1-, 3-, and 5-year OS, respectively) (Fig. 6C). For a more comprehensive evaluation of the prognosis in patients with ccRCC, we incorporated information on gender, age, risk group, TNM stage, and clinical stage to construct a nomogram to forecast the survival probability (Fig. 6D). The OS forecasted by nomogram was consistent with those observed OS in calibration curves (Fig. 6E), indicating that the prediction of the nomogram was accurate. Importantly, the DE_GRG risk model possessed greater superiority of predicting patient survival compared with other clinical traits in decision curve analysis (DCA) curves (Fig. 6F). In summary, these results proved that the nine-DE_GRG-based risk model could be used as an efficiency prognostic model for ccRCC patients.

3.5. Immune infiltration and drug sensitivity in the risk group

Considering that tumor-infiltrating immune cells influence tumor growth [18,19], we analyzed the variance in immune cell infiltration between ccRCC samples from high- and low-risk groups. The proportion of various infiltrating immune cells was determined using "CIBERSORT" (Fig. 7A). Compared with the low-risk group, the high-risk group exhibited increased infiltration of macrophage M0, T cells regulatory (Tregs), and T cells follicular helper, while exhibited decreased infiltration of mast cells resting, macrophage M2, dendritic cells resting, mast cells activated, and dendritic cells activated (Fig. 7B). According to gene set enrichment analysis (GSEA), the genes in the high-risk group were predominantly involved in the PPAR signaling pathway, neuroactive ligand receptor interaction, peroxisome, renin angiotensin system, and valine, leucine and isoleucine degradation (Fig. 7C). Moreover, Cluster A had a significantly smaller risk score than Cluster B (Fig. 7D). We then visualized the association between clusters and risk groups in an alluvial plot and found that Cluster A was mainly associated with the low-risk group and predicted alive prognosis whereas Cluster B was primarily related to the high-risk group (Fig. 7E). To screen for potential ccRCC treatments, the association between the risk groups and the response to commonly used agents for ccRCC was assessed by determining the IC_{50}. As shown in Fig. 7F, the IC_{50} values for gemcitabine, cisplatin, 5-fluorouracil, sabutoclax, and rapamycin in the high-risk group were significantly lower than those in the low-risk group, suggesting that these drugs had better efficacy in patients with high-risk ccRCC.

3.6. FUT6 inhibits ccRCC progression

To further validate the findings from bioinformatics analysis, we used RT-qPCR to assess the expression of nine DE_GRGs in renal epithelial cell line HK-2 and renal cancer cell lines 786-O and Caki-1. However, because of the mismatch between CHST9, HS3ST2, and ST8SIA4 expression and prognosis, they were excluded. As shown in Fig. 8A, the expression of COLGALT1 was significantly increased in 786-O and Caki-1 cells compared with HK-2 cells, while the expression of FUT3, FUT6, POMGNT2, UGT3A1, and UGT8 was significantly decreased. Given that FUT6 had the most significant p-value, it was used for further functional validation. We overexpressed FUT6 in 786-O and Caki-1 cells, and the overexpression efficiency was confirmed by RT-qPCR (Fig. 8B). We found that FUT6 overexpression significantly reduced the proliferation of 786-O and Caki-1 cells compared with the control group (Fig. 8C and D). Transwell results revealed that both the migration and invasion abilities of 786-O and Caki-1 cells in the FUT6 overexpression group were significantly attenuated compared to the control group (Fig. 8E and F). These results indicated that FUT6 suppressed the proliferation, migration, and invasion of ccRCC cells.

4. Discussion

The prognosis of patients with advanced or metastatic ccRCC remains poor. Although the OS has significantly improved in the last 15 years, early diagnosis and risk stratification are crucial to improve the survival time of patients with ccRCC [20]. In our study, ccRCC samples were divided into two subtypes (Clusters A and B) based on DE_GRGs, and they led to significantly different prognoses and immune cell infiltration. Moreover, we identified nine DE_GRGs (CHST9, COLGALT1, FUT3, FUT6, HS3ST2, POMGNT2, ST8SIA4, UGT3A1, and UGT8) that were used to construct robust risk score features. Among them, FUT6 diminished the proliferation, migration, and invasion of ccRCC cells.

Currently, there are some good risk models that are used to predict the prognosis of patients with ccRCC, including cuproptosis-related lncRNA [21] and gene signatures [22], ferroptosis-related lncRNA signature [23], and natural killer cell-related gene signature [24]. A signature based on immune and stromal cell infiltration in the tumor microenvironment was correlated with survival outcomes of ccRCC [25]. A model with 28 ubiquitin–proteasome system-related genes held remarkable prognostic value in ccRCC [26]. A three distant metastasis-associated gene model based on resting mast cells could predict immune response and distant metastasis in ccRCC [27]. These findings indicate that polygenic risk models based on disease genes have great prospects in predicting the prognosis of ccRCC patients. However, only one article on prognostic risk models for glycosylation-related polygenes could be retrieved in public databases. Based on the label-free nLC-ESI MS/MS, Santorelli et al. demonstrated that urinary N-glycoproteome (such as CD97, COCH, P3IP1, APOB, FINC, CERU, CFAH, HPT, and PLTP) is a distinct feature of ccRCC-related progression [28]. In a recent report, Li et al. found that specific protein glycosylation profiles could distinguish a high-risk ccRCC disease subgroup [29]. Unfortunately, they did not construct risk models associated with GRGs to evaluate the prognostic potency of these proteins in ccRCC. In this study, we established a prognostic risk score model based on nine DE_GRGs and proved that it can effectively predict prognosis

of ccRCC patients. Therefore, this study marks the inaugural exploration of the prognostic significance of glycosylation-related polygenes in ccRCC, offering limited evidence to elucidate the pivotal role of glycosylation in ccRCC.

Abnormal glycosylation genes play a crucial role in the initiation, development, and advancement of ccRCC [30]. In our study, the prognostic signature contains nine DE_GRGs, including COLGALT1, FUT3, FUT6, CHST9, HS3ST2, POMGNT2, ST8SIA4, UGT3A1, and UGT8. Among them, COLGALT1 is a galactosyltransferase that can localize endoplasmic-reticulum-derived glycans to collagen [31]. Moreover, COLGALT1 has been reported to be a promising prognostic biomarker of ccRCC and exhibits a correlation with immunotherapy response [32]. FUT3 and FUT6, the enzymes responsible for adding fucose to N-glycans, were significantly reduced in ccRCC tumor tissues compared with the normal tissues [33]. Li et al. proved that high FUT3 expression is associated with poor prognosis of ccRCC, as indicated by shorter OS and recurrence free survival [34]. POMGNT2 is a gatekeeper enzyme for the functional glycosylation of α-dystroglycan [35] and shows a high rate (nearly 90 %) of heterozygosity loss in ccRCC [36], suggesting that ccRCC is particularly sensitive to disruption of dystroglycan function. ST8SIA4 transfers sialic acid (located at the terminal positions of N- and O-linked glycans) to the terminal position of the sugar [37,38]. A previous study found that lncRNA HOTAIR/miR-124/ST8SIA4 enhanced the malignancy of RCC [39]. An IFN-γ response-related signature of seven genes containing ST8SIA4 could effectively predict ccRCC prognosis [40]. UGT3A1 (belonging to UDP N-acetylglucosaminyltransferase) and UGT8 (belonging to UDP-glucuronosyltransferases) are members of the UST family [41]. UGT8 was reported to be significantly reduced in ccRCC tissues relative to normal tissues [42]; however, the trend of UGT3A1 expression in ccRCC remains unknown. These studies strongly suggest the contribution of these seven DE_GRGs in ccRCC progression, underscoring the potential of glycosylation-related gene signatures in predicting ccRCC prognosis. In addition, to these seven DE_GRGs, there are no reports about the involvement of CHST9 and HS3ST2 in glycosylation modification or ccRCC development. However, their contribution is integral in our risk model, implying that they have unknown functions. Therefore, future research should investigate CHST9 and HS3ST2. Overall, the independent functions of the DE_GRGs used in constructing the risk model in this study support the model's overall accuracy.

FUT6, belonging to FUT family, plays a vital part in mutple cancers. For example, Li et al. uncovered that up-regulating FUT6 decreased the proliferation, migration and invasion capability of breast cancer cells [43]. Wang et al. found that overexpression of FUT6 suppressed head and neck squamous cell carcinoma cell proliferation, migration and invasion [44]. In agreement with these studies, we discovered that FUT6 repressed the proliferation, migration and invasion of ccRCC cells. Together, FUT6 may be a promising therapeutic target for ccRCC.

Our study has several limitations. First, the prognostic signature containing nine DE_GRGs was confirmed by public databases and needs to be further verified by clinical samples. Second, FUT6 was associated with immune infiltration, but its specific role requires further exploration. Moreover, its antitumor effects and mechanism in ccRCC need to be determined through in vivo experiments.

In conclusion, we developed a prognostic signature based on nine DE_GRGs (CHST9, COLGALT1, FUT3, FUT6, HS3ST2, POMGNT2, ST8SIA4, UGT3A1, and UGT8), demonstrating independent prognostic significance in ccRCC. Interestingly, FUT6 was found to suppress the proliferation, migration, and invasion of ccRCC cells. Our study may provide new directions for predicting the prognosis and survival of patients with ccRCC and help accelerate the development of targeted therapies for ccRCC.

CRediT authorship contribution statement

Wanlei Sun: Writing – original draft, Data curation, Conceptualization. **Long Guo:** Writing – original draft, Formal analysis. **Jianqing Ye:** Writing – original draft, Formal analysis. **Min Zhou:** Writing – original draft, Formal analysis. **Cong Shu:** Validation, Investigation. **Xin Ying:** Validation, Investigation. **Hongliang Liu:** Validation, Investigation. **Fei Liu:** Writing – review & editing, Project administration, Funding acquisition.

Ethics approval and consent to participate

Not applicable.

Consent for publication

Not applicable.

Data availability

The data sets used and/or analyzed during the current study are available from the corresponding author on reasonable request.

Funding

This study was supported by the National Natural Science Foundation of China (82060463 and 82360471) and the Project of the Jiangxi Provincial Department of Science and Technology (20224BAB206060).

Declaration of competing interest

The authors declare that they have no known competing financial interests or personal relationships that could have appeared to

influence the work reported in this paper.

Acknowledgements

Not applicable.

Appendix A. Supplementary data

Supplementary data to this article can be found online at https://doi.org/10.1016/j.heliyon.2024.e39258.

References

[1] R. Wu, K. Wang, Y. Gai, M. Li, J. Wang, C. Wang, et al., Nanomedicine for renal cell carcinoma: imaging, treatment and beyond, J. Nanobiotechnol. 21 (2023) 3, https://doi.org/10.1186/s12951-022-01761-7.
[2] J. Jin, Y. Xie, J.S. Zhang, J.Q. Wang, S.J. Dai, W.F. He, et al., Sunitinib resistance in renal cell carcinoma: from molecular mechanisms to predictive biomarkers, Drug Resist. Updat. 67 (2023) 100929, https://doi.org/10.1016/j.drup.2023.100929.
[3] S.A. Padala, A. Kallam, Clear cell renal carcinoma, in: StatPearls [Internet], StatPearls Publishing, 2021.
[4] H.A. Drabkin, R.M. Gemmill, Cholesterol and the development of clear-cell renal carcinoma, Curr. Opin. Pharmacol. 12 (2012) 742–750, https://doi.org/10.1016/j.coph.2012.08.002.
[5] N.R. Jang, J. Baek, Y. Ko, P.H. Song, M.J. Gu, High MCM6 expression as a potential prognostic marker in clear-cell renal cell carcinoma, V ivo 35 (2021) 299–306, https://doi.org/10.21873/invivo.12259.
[6] L. Gao, J. Xue, X. Liu, L. Cao, R. Wang, L. Lei, A risk model based on autophagy-related lncRNAs for predicting prognosis and efficacy of immunotherapy and chemotherapy in gastric cancer patients, Aging 13 (2021) 25453–25465, https://doi.org/10.18632/aging.203765.
[7] B.H. Zhang, J. Yang, L. Jiang, T. Lyu, L.X. Kong, Y.F. Tan, et al., Development and validation of a 14-gene signature for prognosis prediction in hepatocellular carcinoma, Genomics 112 (2020) 2763–2771, https://doi.org/10.1016/j.ygeno.2020.03.013.
[8] P. Cao, M. Chen, T. Zhang, Q. Zheng, M. Liu, A sialyltransferases-related gene signature serves as a potential predictor of prognosis and therapeutic response for bladder cancer, Eur. J. Med. Res. 28 (2023) 515, https://doi.org/10.1186/s40001-023-01496-7.
[9] Y. Pan, L. Lin, F. Yu, J. Sun, G. Bai, X. He, et al., Cysteine mutations impair the structural stability of phosphomannomutase 2 (PMM2) in glycosylation-associated metabolic disorders, Genes Dis 10 (2023) 1743–1746, https://doi.org/10.1016/j.gendis.2022.10.002.
[10] H. Wu, X. Zhao, T. Zhu, D. Rong, Y. Wang, D. Leng, et al., A glycosyltransferase-related signature for predicting overall survival in head and neck squamous cell carcinoma, Front. Genet. 13 (2022) 856671, https://doi.org/10.3389/fgene.2022.856671.
[11] J. Eichler, Protein glycosylation, Curr. Biol. 29 (2019) R229–R231, https://doi.org/10.1016/j.cub.2019.01.003.
[12] A. Silsirivanit, Glycosylation markers in cancer, Adv. Clin. Chem. 89 (2019) 189–213.
[13] S.S. Pinho, C.A. Reis, Glycosylation in cancer: mechanisms and clinical implications, Nat. Rev. Cancer 15 (2015) 540–555, https://doi.org/10.1038/nrc3982.
[14] C. Liu, Z. Li, L. Xu, Y. Shi, X. Zhang, S. Shi, et al., GALNT6 promotes breast cancer metastasis by increasing mucin-type O-glycosylation of alpha2M, Aging 12 (2020) 11794–11811, https://doi.org/10.18632/aging.103349.
[15] Y.D. Chu, T.C. Fan, M.W. Lai, C.T. Yeh, GALNT14-mediated O-glycosylation on PHB2 serine-161 enhances cell growth, migration and drug resistance by activating IGF1R cascade in hepatoma cells, Cell Death Dis. 13 (2022) 956, https://doi.org/10.1038/s41419-022-05419-y.
[16] H. Zhang, Y. Liu, H. Xie, Q. Fu, Z. Liu, Y. Zhu, et al., Beta-1,4-galactosyltransferase II predicts poor prognosis of patients with non-metastatic clear-cell renal cell carcinoma, Tumour Biol 39 (2017) 1010428317691417, https://doi.org/10.1177/1010428317691417.
[17] Q. Bai, L. Liu, W. Xi, J. Wang, Y. Xia, Y. Qu, et al., Prognostic significance of ST6GalNAc-1 expression in patients with non-metastatic clear cell renal cell carcinoma, Oncotarget 9 (2018) 3112–3120, https://doi.org/10.18632/oncotarget.11258.
[18] K. Pang, Z.D. Shi, L.Y. Wei, Y. Dong, Y.Y. Ma, W. Wang, et al., Research progress of therapeutic effects and drug resistance of immunotherapy based on PD-1/PD-L1 blockade, Drug Resist. Updat. 66 (2023) 100907, https://doi.org/10.1016/j.drup.2022.100907.
[19] Y. Li, S. Li, Z. Jiang, K. Tan, Y. Meng, D. Zhang, et al., Targeting lymph node delivery with nanovaccines for cancer immunotherapy: recent advances and future directions, J. Nanobiotechnol. 21 (2023) 212, https://doi.org/10.1186/s12951-023-01977-1.
[20] S. Demasure, I. Spriet, P.R. Debruyne, A. Laenen, W. Wynendaele, M. Baldewijns, et al., Overall survival improvement in patients with metastatic clear-cell renal cell carcinoma between 2000 and 2020: a retrospective cohort study, Acta Oncol 61 (2022) 22–29, https://doi.org/10.1080/0284186X.2021.1989720.
[21] Z. Bai, J. Lu, A. Chen, X. Zheng, M. Wu, Z. Tan, et al., Identification and validation of cuproptosis-related LncRNA signatures in the prognosis and immunotherapy of clear cell renal cell carcinoma using machine learning, Biomolecules 12 (2022), https://doi.org/10.3390/biom12121890.
[22] K. Zhang, W. Yang, Z. Zhang, K. Ma, L. Li, Y. Xu, et al., A novel cuproptosis-related prognostic model and the hub gene FDX1 predict the prognosis and correlate with immune infiltration in clear cell renal cell carcinoma, J. Oncol. 2022 (2022) 2124088, https://doi.org/10.1155/2022/2124088.
[23] S.Y. Wei, B. Feng, M. Bi, H.Y. Guo, S.W. Ning, R. Cui, Construction of a ferroptosis-related signature based on seven lncRNAs for prognosis and immune landscape in clear cell renal cell carcinoma, BMC Med. Genom. 15 (2022) 263, https://doi.org/10.1186/s12920-022-01418-2.
[24] X. Shi, M. Yuan, Y. Yang, N. Wang, Y. Niu, C. Yang, et al., Prognostic model for clear-cell renal cell carcinoma based on natural killer cell-related genes, Clin. Genitourin. Cancer (2022), https://doi.org/10.1016/j.clgc.2022.11.009.
[25] J. Luo, Y. Xie, Y. Zheng, C. Wang, F. Qi, J. Hu, et al., Comprehensive insights on pivotal prognostic signature involved in clear cell renal cell carcinoma microenvironment using the ESTIMATE algorithm, Cancer Med. 9 (2020) 4310–4323, https://doi.org/10.1002/cam4.2983.
[26] H. Guo, Y. Li, Y. Liu, L. Chen, Z. Gao, L. Zhang, et al., Prognostic role of the ubiquitin proteasome system in clear cell renal cell carcinoma: a bioinformatic perspective, J. Cancer 12 (2021) 4134–4147, https://doi.org/10.7150/jca.53760.
[27] Y. Su, T. Zhang, J. Lu, L. Qian, Y. Fei, L. Zhang, et al., Identification and validation of the prognostic panel in clear cell renal cell carcinoma based on resting mast cells for prediction of distant metastasis and immunotherapy response, Cells 12 (2023), https://doi.org/10.3390/cells12010180.
[28] L. Santorelli, G. Capitoli, C. Chinello, I. Piga, F. Clerici, V. Denti, et al., In-depth mapping of the urinary N-glycoproteome: distinct signatures of ccRCC-related progression, Cancers 12 (2020), https://doi.org/10.3390/cancers12010239.
[29] Y. Li, T.M. Lih, S.M. Dhanasekaran, R. Mannan, L. Chen, M. Cieslik, et al., Histopathologic and proteogenomic heterogeneity reveals features of clear cell renal cell carcinoma aggressiveness, Cancer Cell 41 (2023) 139–163 e117, https://doi.org/10.1016/j.ccell.2022.12.001.
[30] X. Zhu, A. Al-Danakh, L. Zhang, X. Sun, Y. Jian, H. Wu, et al., Glycosylation in renal cell carcinoma: mechanisms and clinical implications, Cells 11 (2022), https://doi.org/10.3390/cells11162598.
[31] T. Hennet, Collagen glycosylation, Curr. Opin. Struct. Biol. 56 (2019) 131–138, https://doi.org/10.1016/j.sbi.2019.01.015.
[32] S. Liu, Y. Yu, Y. Wang, B. Zhu, B. Han, COLGALT1 is a potential biomarker for predicting prognosis and immune responses for kidney renal clear cell carcinoma and its mechanisms of ceRNA networks, Eur. J. Med. Res. 27 (2022) 122, https://doi.org/10.1186/s40001-022-00745-5.
[33] R.R. Drake, C. McDowell, C. West, F. David, T.W. Powers, T. Nowling, et al., Defining the human kidney N-glycome in normal and cancer tissues using MALDI imaging mass spectrometry, J. Mass Spectrom. 55 (2020) e4490, https://doi.org/10.1002/jms.4490.

[34] L. Meng, L. Xu, Y. Yang, L. Zhou, Y. Chang, T. Shi, et al., High expression of FUT3 is linked to poor prognosis in clear cell renal cell carcinoma, Oncotarget 8 (2017) 61036–61047, https://doi.org/10.18632/oncotarget.17717.
[35] S.M. Halmo, D. Singh, S. Patel, S. Wang, M. Edlin, G.J. Boons, et al., Protein O-linked mannose beta-1,4-N-Acetylglucosaminyl-transferase 2 (POMGNT2) is a gatekeeper enzyme for functional glycosylation of alpha-dystroglycan, J. Biol. Chem. 292 (2017) 2101–2109, https://doi.org/10.1074/jbc.M116.764712.
[36] M.R. Miller, D. Ma, J. Schappet, P. Breheny, S.L. Mott, N. Bannick, et al., Downregulation of dystroglycan glycosyltransferases LARGE2 and ISPD associate with increased mortality in clear cell renal cell carcinoma, Mol. Cancer 14 (2015) 141, https://doi.org/10.1186/s12943-015-0416-z.
[37] R.A. Somerville, Host and transmissible spongiform encephalopathy agent strain control glycosylation of PrP, J. Gen. Virol. 80 (Pt 7) (1999) 1865–1872, https://doi.org/10.1099/0022-1317-80-7-1865.
[38] M. Audry, C. Jeanneau, A. Imberty, A. Harduin-Lepers, P. Delannoy, C. Breton, Current trends in the structure-activity relationships of sialyltransferases, Glycobiology 21 (2011) 716–726, https://doi.org/10.1093/glycob/cwq189.
[39] Y. Pan, Y. Wu, J. Hu, Y. Shan, J. Ma, H. Ma, et al., Long noncoding RNA HOTAIR promotes renal cell carcinoma malignancy through alpha-2, 8-sialyltransferase 4 by sponging microRNA-124, Cell Prolif. 51 (2018) e12507, https://doi.org/10.1111/cpr.12507.
[40] L. Liu, X. Du, J. Fang, J. Zhao, Y. Guo, Y. Zhao, et al., Development of an interferon gamma response-related signature for prediction of survival in clear cell renal cell carcinoma, J. Inflamm. Res. 14 (2021) 4969–4985, https://doi.org/10.2147/JIR.S334041.
[41] R. Meech, D.-G. Hu, J. Miners, P. Mackenzie, UDP-glycosyltransferases. Comprehensive Toxicology, Third Edition, 2018, pp. 468–496.
[42] W.-J. Park, J.Y. Park, T.K. Kwon, J.-W. Park, S. Kim, In silico analysis for sphingolipid metabolism-related genes in human kidney clear cell carcinoma using the cancer genome Atlas, Keimyung Med. J. 39 (2020) 14–22, https://doi.org/10.46308/kmj.2020.00101.
[43] N. Li, Y. Liu, Y. Miao, L. Zhao, H. Zhou, L. Jia, MicroRNA-106b targets FUT6 to promote cell migration, invasion, and proliferation in human breast cancer, IUBMB Life 68 (2016) 764–775, https://doi.org/10.1002/iub.1541.
[44] Q. Wang, C. Liao, Z. Tan, X. Li, X. Guan, H. Li, et al., FUT6 inhibits the proliferation, migration, invasion, and EGF-induced EMT of head and neck squamous cell carcinoma (HNSCC) by regulating EGFR/ERK/STAT signaling pathway, Cancer Gene Ther. 30 (2023) 182–191, https://doi.org/10.1038/s41417-022-00530-w.